Stress-induced flow heterogeneity on the bedding plane of a layered fractured rock

Conference Paper

Author(s):
Lei, Qinghua (iD); Wang, Xiaoguang; Kang, Peter; Latham, John-Paul; Tsang, Chin-Fu

Stress-Induced Flow Heterogeneity on the Bedding Plane of Fractured Layered Rock

Qinghua Lei [a], Xiaoguang Wang [b], Peter Kang [c], John-Paul Latham [d], Chin-Fu Tsang [e,f]

[a] Department of Earth Sciences, ETH Zürich, Zürich, Switzerland
[b] Laboratoire HydroSciences Montpellier, Université de Montpellier, Montpellier, France
[c] Department of Earth Sciences, University of Minnesota, Minneapolis, USA
[d] Department of Earth Science and Engineering, Imperial College London, London, UK
[e] Department of Earth Sciences, Uppsala University, Uppsala, Sweden
[f] Energy Geosciences Division, Lawrence Berkeley National Laboratory, Berkeley, USA
e-mails: qinghua.lei@erdw.ethz.ch (Q. Lei), xiaoguang.wang@umontpellier.fr (X. Wang),
pkkang@umn.edu (P.K. Kang), j.p.latham@imperial.ac.uk (J.-P. Latham), cftsang@lbl.gov (C.-F. Tsang)

1 Introduction

The understanding of groundwater flow in sedimentary geological formations is of great interests for drinking water extraction and contaminant remediation. When meteoric water infiltrates through a sequence of fractured strata driven by gravitational forces, the flow is redistributed by the laterally extensive bedding planes when the water attempts to enter a lower layer from its upper layer via the bedding interface. Heterogeneous flow may emerge on the bedding plane, depending on the distribution of fractures in the neighbouring layers and the aperture contrast between the interlayer bedding and intralayer fractures [1]. On account of the stress-dependent nature of bedding/fracture apertures [2], we expect that the flow pattern on the bedding plane is also affected by geomechanical processes such as compression-induced closure and shear-induced dilation of these discontinuities. In this paper, we conduct three-dimensional (3D) numerical simulation to investigate this problem and gain insights into the emergence of heterogeneous fluid flow on bedding planes, which is strongly related to the initiation of karst features in sedimentary rocks [3].

2 Fractured Layered Rock

We construct three-dimensional (3D) dual-layer structural models (Figure 1) to represent typical sections of sedimentary sequence. The model consists of vertically-overlaid two strata with a bedding plane sandwiched in between. Each cuboid-shaped layer is 0.05 m thick with both lateral dimensions equal to 2 m. The strata-bound, bed-normal fractures of the upper layer are independent of the fractures of the lower layer. These fractures follow a power-law length distribution whose density function is given as $n(l) = Cl^{-a}$, with $l_{\min} \leq l \leq l_{\max}$, where l is the fracture length, a is the power-law length exponent and C is a constant term related to fracture density. The maximum and minimum fracture lengths are given as $l_{\min} = L/20 = 0.05$ m and $l_{\max} = 20L = 40$ m, respectively. The location and strike direction of fractures are assumed purely random. We fix the fracture intensity of each layer (ratio of the total surface area of fractures to the rock volume) to be identical as $P_{32} = 5$ m^{-1}, and explore three different length exponent cases, i.e. $a = 1.5$, 2.5, and 3.5. When a is small, the fracture network in each distinct bed is dominated by very large fractures; when a is large, the fracture network mainly consists of small fractures (Figure 1).
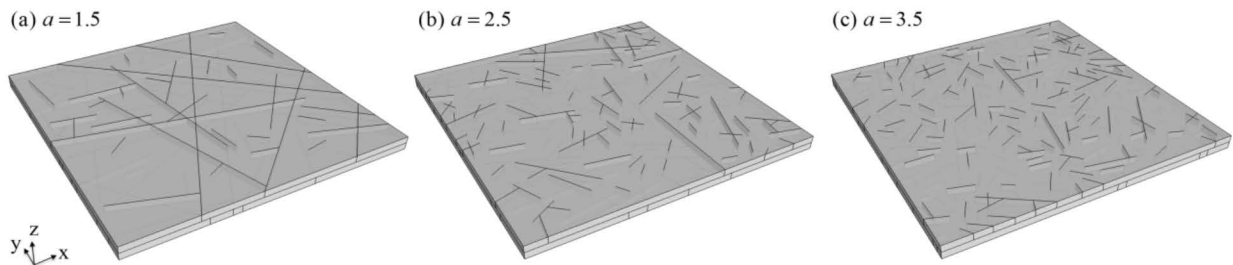

Figure 1. The structural model of fractured layered rocks (2 m × 2 m × 0.1 m) embedded with fracture networks having different power-law length exponents $a = 1.5$, 2.5 and 3.5.

3 Hydromechanical Modelling

The geomechanical response of the fractured layered rock is simulated using a 3D hybrid finite-discrete element model [2,4], which can capture the deformation of intact rocks, interaction of matrix blocks, variability of local stresses, displacement of pre-existing fractures, and propagation of new cracks.

The closure of the bedding plane/fractures under normal compression is calculated based on a hyperbolic formulation [5] given as:

$$v_n = \frac{\sigma_n v_m}{k_{n0} v_m + \sigma_n},$$ (1)

where v_n is the normal closure, σ_n is the effective normal compressive stress, k_{n0} is the initial normal stiffness, and v_m is the maximum allowable closure. The shear deformation of discontinuities is calculated based on an elasto-plastic constitutive model with strain-softening [6]. In the elastic phase, the shear stress τ increases linearly with the shear displacement u and the slope of the stress-displacement curve is given by the shear stiffness k_s. During this stage, the opposing discontinuity walls ride over each other's asperities, resulting in dilational displacement. The peak shear stress τ_p is eventually reached when the displacement arrives at the peak shear displacement u_p, beyond which the asperities begin to shear off and irreversible damage starts to occur. If the discontinuity continues to slide, the shear stress decreases linearly to the residual shear stress τ_r, during which the asperities are crushed but dilation continues. Finally, after the displacement exceeds the residual displacement u_r, the shear stress remains constant (i.e. $\tau = \tau_r$) and no further dilation develops. In this model, the peak shear stress τ_p is calculated as [7]:

$$\tau_p = \sigma_n \tan(\phi_b + \phi_i)(1 - a_s) + a_s c,$$ (2)

where a_s is the proportion of total fracture area sheared through asperities, ϕ_i is the dilation angle, c is the shear strength of the asperity (i.e. cohesion of the intact rock), and ϕ_b is the basic friction angle substituted using the residual friction angle ϕ_r [8]. a_s and ϕ_i are respectively given as [7]:

$$a_s = 1 - \left(1 - \frac{\sigma_n}{\sigma_u}\right)^{m_1},$$ (3)

$$\tan \phi_i = \begin{cases} \left(1 - \frac{\sigma_n}{\sigma_u}\right)^{m_2} \tan \phi_{i0}, & \text{for } u \le u_r, \\ 0, & \text{for } u > u_r \end{cases}$$ (4)

where ϕ_{i0} is the initial dilation angle when $\sigma_n = 0$, and m_1 and m_2 are empirical parameters with suggested values of 1.5 and 4.0, respectively. The residual shear stress τ_r is given as [8]:

$$\tau_r = \sigma_n \tan \phi_r.$$ (5)

The dilational displacement v_s is related to the shear displacement u in an incremental form as [7]:

$$dv_s = -\tan \phi_i du,$$ (6)

The fracture aperture h under coupled normal and shear loadings is thus derived as [4]:

$$h = \begin{cases} h_0 + w, & \sigma_n < 0 \\ h_0 - v_n - v_s, & \sigma_n \ge 0 \end{cases},$$ (7)

where h_0 is the initial aperture, and w is the separation of opposing walls if the discontinuity is under tension. The local bedding plane/fracture permeability is then calculated as $h^2/12$ based on the cubic law.

Fluid flow through the geomechanically-loaded fractured stratified rock is solved using the finite element method [1]. The top and bottom of the model are imposed with a fixed pressure drop (i.e. 1kPa), while the four orthogonal boundaries parallel to the flow direction are impervious.

Material properties of the fractured layered rocks are assumed as follows. The bulk density is 2700 kg/m^3, the matrix permeability is 10^{-17} m^2, the Young's modulus is 30.0 GPa, the Poisson's ratio is 0.27, the internal friction angle is 27˚, the tensile strength is 15.0 MPa, the cohesive strength is 30.0 MPa, and the mode I and II energy release rates are 146.9 and 174.7 J/m^2, respectively. A constant initial aperture, i.e. 0.05 mm, is assigned to all discontinuities. The maximum allowable closure is 0.045 mm, the initial normal stiffness is 10.0 GPa/m, the residual friction angle is 25˚, the peak shear displacement is 1.0 mm, the residual shear displacement is 3.0 mm, and the initial dilation angle is 10˚. Effective far-field stresses are loaded orthogonally to the domain, and five different stress scenarios are explored covering from typical to very extreme conditions to bring out clearly the system behaviour: (i) $S_x = S_z = 1$ MPa, (ii) $S_x = 1$ MPa, $S_z = 3$ MPa, (iii) $S_x = 3$ MPa, $S_z = 1$ MPa, (iv) $S_x = 1$ MPa, $S_z = 5$ MPa, and (v) $S_x = 5$ MPa, $S_z = 1$ MPa, while $S_y \equiv 1$ MPa.

4 Results and Discussions

$S_y \equiv 1$ MPa	$S_x = 1$ MPa $S_z = 1$ MPa	$S_x = 1$ MPa $S_z = 3$ MPa	$S_x = 1$ MPa $S_z = 5$ MPa	$S_x = 3$ MPa $S_z = 1$ MPa	$S_x = 5$ MPa $S_z = 1$ MPa

Aperture (mm)
0.005 0.01 0.015 0.02 0.025 0.03
0.5 m

Flow rate (m³/s)
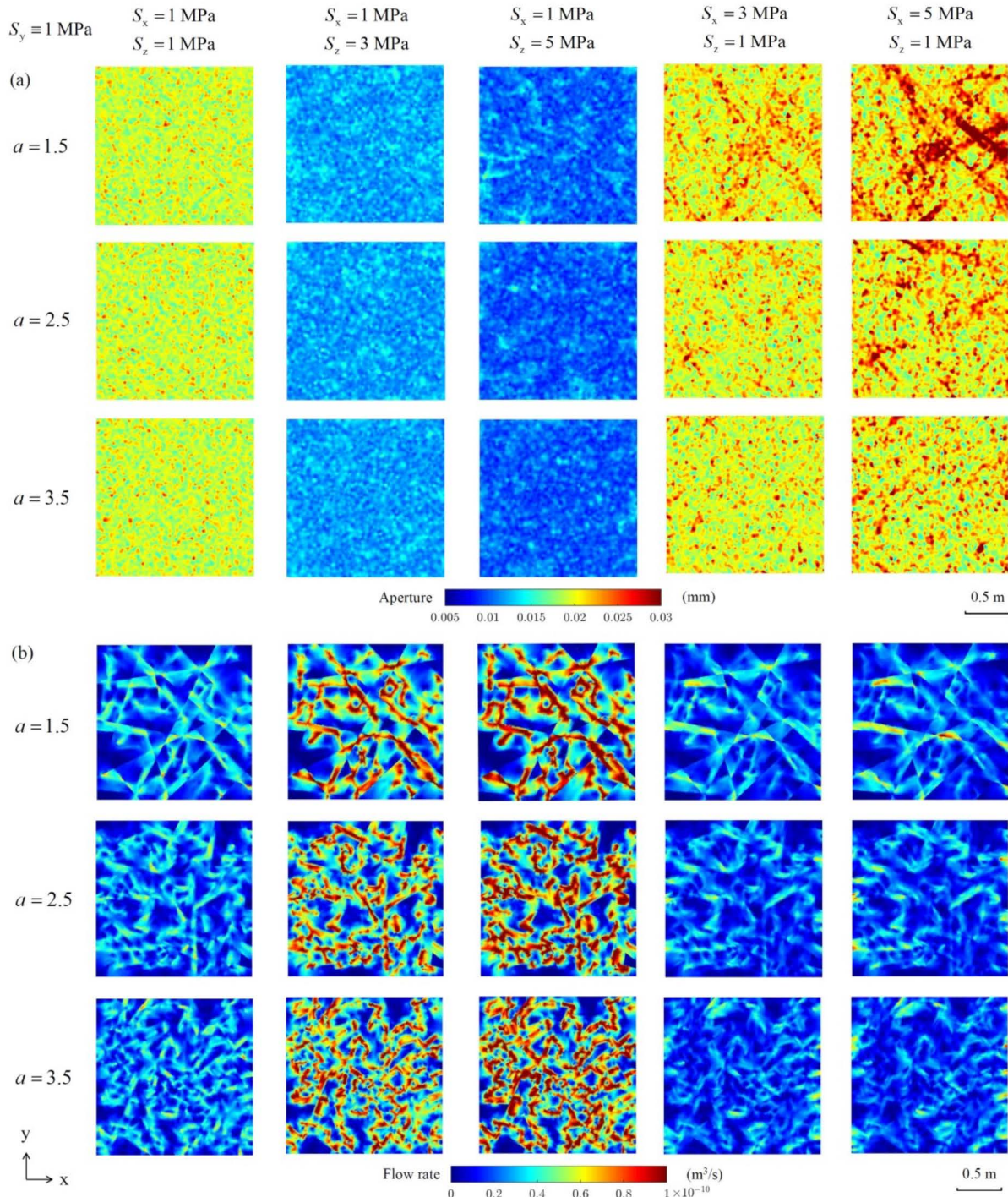0 0.2 0.4 0.6 0.8 1×10^{-10}
0.5 m

Figure 2. The distribution of (a) apertures and (b) flow rates on the bedding plane under different stress conditions.

Figure 2 shows the distribution of apertures and flow rates on the bedding plane of the fracture layered rocks under different stress conditions. Figure 3 further illustrates the variation of the bedding plane aperture, h_b, and the fracture aperture, h_f, in response to stress loading. When the system is under an isotropic stress field, h_b exhibits a quite homogenous distribution (although small variation exists possibly due to the presence of intersecting fractures that dissect the layer into blocks and the bedding plane into patches) (Figure 2a) with a mean reduced from the initial value of 0.05 mm to about 0.02 mm under normal compression (Figure 3a), which is also in general identical to h_f (Figure 3b). However, the flow

pattern on the bedding plane exhibits inhomogeneous characteristics, which are attributed to the local distribution of fracture-bedding intersection lines, i.e. the inflow/outflow boundaries on the bedding plane. High flow rate is concentrated in the region that efficiently transmits fluids from the upper-bed fractures to the lower-bed ones, i.e. shortest paths linking the inflow to outflow. Furthermore, the flow field becomes more diffuse as a increases, as a result of the spreading of short intersection traces on the bedding plane. When S_z increases and S_x is fixed, h_b is considerably reduced under the enhanced normal stress (Figures 2a & 3a). The increase of h_f (Figure 3b) is caused by vertical shearing of some bed-normal fractures (when two fractures of different beds are close to each other, they tend to macroscopically form a slip zone oblique to S_z accommodating intense dislocation and rotation). Thus, the ratio of h_b/h_f significantly decreases (Figure 3c), leading to stronger dependence of bedding plane flow on the geometrical distribution of intersection lines, such that the flow becomes highly heterogeneous. When S_x increases and S_z is fixed, large apertures emerge on the bedding plane, because the sliding along preferentially-oriented, large fractures under the enhanced horizontal differential stress also causes pronounced shearing and dilatancy on the bedding plane. Thus, in the case of $a = 1.5$ (dominated by large fractures), greater h_f (Figure 3b) and more heterogeneously distributed h_b (Figure 2a) are generated; however, in the other two cases, shearing along short fractures is suppressed by matrix resistance and more fracture closure occurs under the elevated horizontal stress level. Surprisingly, only minor changes appear in the flow field on the bedding plane as S_x increases. This is due to the strong dependence of bedding plane flow on h_b/h_f, which only exhibits a small variation (Figure 3c).

To sum up, one key finding of this research is that the emergence of flow heterogeneity on the bedding plane as water vertically infiltrates through a fractured stratified system is mainly caused by the stress-induced aperture contrast between the bedding plane and bed-normal fractures under polyaxial stress loading, whereas the stress-induced aperture heterogeneity on the bedding plane itself only has a minor impact. Future work includes the exploration of higher stress regimes (i.e. greater depth scenarios) and modelling of karstification processes based on hydro-mechanical-chemical simulations.
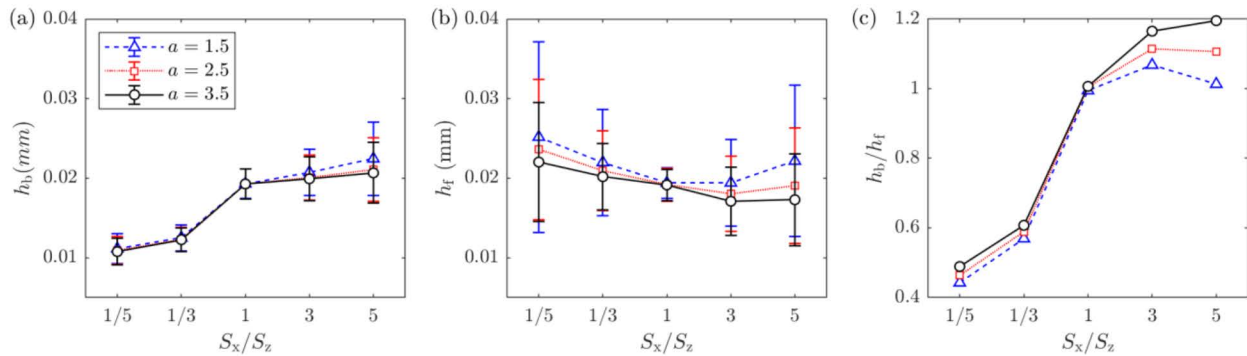

Figure 3. Variation of (a) the bedding plane aperture h_b and (b) the fracture aperture h_f as well as (c) their ratio. The marker in (a) and (b) represents the mean aperture of all segments and the error bars indicate the standard deviation.

References

[1] Wang X, Lei Q, Lonergan L, Jourde H, Gosselin O, Cosgrove J. Heterogeneous fluid flow in fractured layered carbonates and its implication for generation of incipient karst. *Adv Water Resour*. 2017;107:502–516.

[2] Lei Q, Latham J-P, Xiang J, Tsang C-F. Polyaxial stress-induced variable aperture model for persistent 3D fracture networks. *Geomech Energy Environ*. 2015;1:34–47.

[3] Palmer AN. Origin and morphology of limestone caves. *Geol Soc Am Bull*. 1991;103:1–21.

[4] Lei Q, Wang X, Xiang J, Latham J-P. Polyaxial stress-dependent permeability of a three-dimensional fractured rock layer. *Hydrogeol J*. 2017;25:2251–2262.

[5] Bandis SC, Lumsden AC, Barton NR. Fundamentals of rock joint deformation. *Int J Rock Mech Min Sci Geomech Abstr*. 1983;20:249–268.

[6] Goodman RE. *Methods of Geological Engineering*. St Paul: West Publishing; 1976.

[7] Saeb S, Amadei B. Modelling rock joints under shear and normal loading. *Int J Rock Mech Min Sci Geomech Abstr*. 1992;29:267–278.

[8] Barton N, Choubey V. The shear strength of rock joints in theory and practice. *Rock Mech*. 1977;10:1–54.